

Weierstraß-Institut
für Angewandte Analysis und Stochastik
Leibniz-Institut im Forschungsverbund Berlin e. V.

Preprint

ISSN 2198-5855

**Semiconductor mode-locked lasers with coherent dual mode
optical injection: simulations, analysis and experiment**

Rostislav M. Arkhipov¹, Tatiana Habruseva^{2,3}, Alexander Pimenov⁴,
Mindaugas Radziunas⁴, Guillaume Huyet^{1,2,3}, Andrei G. Vladimirov^{4,5}

submitted: November 30, 2015

¹ Saint Petersburg National Research University of
Information Technologies, Mechanics and Optics
199034 St Petersburg, Russia
E-Mail: arkipovrostislav@gmail.com

² Tyndall National Institute
University College Cork
Lee Maltings, Dyke Parade, Cork, Ireland

³ Centre for Advanced Photonics and Process Analysis
Cork Institute of Technology
Cork, Ireland

⁴ Weierstrass Institute
Mohrenstr. 39, 10117, Berlin, Germany
E-Mail: alexander.pimenov@wias-berlin.de
mindaugas.radziunas@wias-berlin.de
andrei.vladimirov@wias-berlin.de

⁵ Lobachevsky State University of Nizhny Novgorod
Nizhny Novgorod, Russia

No. 2184

Berlin 2015



2010 *Physics and Astronomy Classification Scheme*. 42.55.Px, 42.60.Fc, 42.60.Lh.

Key words and phrases. Passively mode-locked semiconductor lasers, dual frequency optical injection, locking.

R.A., M.R., G.H., and A.G.V. would like to acknowledge the support of EU FP7 ITN PROPHET, Grant No. 264687. A.P. and A.G.V. acknowledge the support from SFB 787 of the DFG. T.H. acknowledges the support of IRC Government of Ireland postdoctoral fellowship, grant GOIPD/2014/228 (TUSELAMO). A.G.V. acknowledges the support of the Science Foundation Ireland E.T.S. Walton Visitors Award Programme under Contract No. 11/W.1/I2073 and of the grant 14-41-00044 of Russian Scientific Foundation. This work was partially financially supported by Government of Russian Federation, Grant 074-U01.

Edited by
Weierstraß-Institut für Angewandte Analysis und Stochastik (WIAS)
Leibniz-Institut im Forschungsverbund Berlin e. V.
Mohrenstraße 39
10117 Berlin
Germany

Fax: +49 30 20372-303
E-Mail: preprint@wias-berlin.de
World Wide Web: <http://www.wias-berlin.de/>

Abstract

Using a delay differential equations model we study the dynamics of a passively mode-locked semiconductor laser with dual frequency coherent optical injection. The locking regions where the laser pulse repetition rate is synchronized to the separation of the two injected frequencies were calculated numerically and measured experimentally. Asymptotic analysis performed in the limit of the small injection field amplitude revealed the dependence of the locking regions on the model parameters, such as optical bandwidth, absorber recovery time and linear losses.

1 Introduction

Passively mode-locked (PML) semiconductor lasers are cost efficient sources of short optical pulses with high repetition rates ranging from a few to hundreds of GHz [1]. Development of stabilized semiconductor light sources is in a great demand for a wide range of applications, such as optical telecommunications, frequency metrology, optical sampling, and clock recovery [2–5]. The optical spectrum of such lasers is a frequency comb with line spacing equal to the pulse repetition rate. Due to the spontaneous emission noise and some technical factors these lasers exhibit significant timing jitter, which limits their performance in a number of applications. For stabilization of the pulse repetition frequency external radio-frequency (RF) modulation of the reverse bias applied to the laser absorber section is used [6]. When the frequency of the modulation is sufficiently close to the repetition rate, f_0 , of the free running PML semiconductor laser, the pulse repetition rate synchronizes with this frequency. Such technique is called “hybrid mode-locking” [7–13].

Hybrid mode-locked lasers were studied experimentally in [8, 12, 13, 15] and theoretically in [13, 16]. It was demonstrated that the locking range increased almost linearly with the modulation amplitude and with the absolute value of the reverse bias applied to the absorber section. Furthermore, it was shown in Ref. [16], both theoretically and experimentally, that hybrid mode-locking can be also achieved when the frequency of the external modulation is approximately twice smaller than the pulse repetition frequency of a free-running laser, f_0 .

An efficient approach to improve characteristics of pulses emitted by PML lasers is based on the use of optical injection from a single mode master laser [17–21]. When one of the slave laser modes is locked to the external single frequency signal, the slave laser phase noise is reduced [18], undesired waveform instabilities are suppressed [20], and slave laser optical spectrum is narrowed [17, 18]. However, single mode injection does not allow to control the repetition rate of mode-locked pulses [17, 21]. On the other hand, neither hybrid nor active mode-locking techniques influence the frequency noise of an individual line in the frequency comb [22, 23].

An alternative approach to timing jitter suppression in PML lasers is based on the use of coherent dual mode optical injection [14]. Here, a coherent output from a CW laser is sent through a Mach-Zehnder amplitude modulator producing two coherent sidebands with a suppressed carrier frequency. These two sidebands are then injected into the PML laser. High quality optical

frequency combs with narrow lines and small RF beating noise can be generated by injecting two coherent tones into PML lasers. Semiconductor lasers with dual mode optical injection were studied experimentally in [14, 22, 23]. It was shown that synchronization to coherent tones resulted in both jitter and individual modal line width reduction for all locked modes.

In the present paper, using a set of delay differential equations similar to that derived in [24–26], we perform a theoretical analysis of the dynamics of a dual mode optically injected PML laser. We calculate numerically and estimate asymptotically the width of the locking range as a function of the injected field power and model parameters for the two following cases. In the first case the frequency separation between two injected frequencies was varied at the fixed master laser frequency. We will refer to the locking range obtained in this case as RF locking range. In the second case the locking range was calculated by changing the master laser frequency while keeping the value of the modulation frequency constant and equal (or multiple) to the pulse repetition frequency of the free-running PML laser. We will call the locking range obtained in this way the optical locking range. We also present the results of the experimental study of the effect of dual mode optical injection on a 10-GHz PML quantum dot semiconductor laser. We demonstrate theoretically and experimentally that the optical locking range can be much wider than the RF locking range. We show that the optical locking range calculated numerically for nonzero linewidth enhancement factors is wider than that obtained for zero linewidth enhancement factors and reaches the values, which are in qualitative agreement with experimental observations.

The structure of the paper is as follows. In Section 2 we introduce the model equations for an optically injected PML laser and perform numerical estimation of the optical and RF locking ranges. In Section 3 we discuss the results of the experimental study of a 10-GHz quantum dot PML laser with dual mode optical injection. In Section 4 we perform an asymptotic analysis of the model equations in the limit of small injection field amplitudes and obtain estimates for the locking range width, which we use to analyse the dependence of the two locking ranges on different model parameters. Concluding remarks are given in Section 5.

2 Model equations

Our analysis is based on a set of delay differential equations (DDE) describing time evolution of the electric field amplitude at the entrance of the laser absorber section $A(t)$, as well as saturable gain $G(t)$, and saturable absorption $Q(t)$ in the gain and absorber sections of the device, respectively. The DDE model was first derived in [24–26] and further generalized in [27] under the approximation of unidirectional lasing in a ring cavity and Lorentzian shape of the spectral filtering element. In the case of externally injected mode-locked laser this model can be written in the following form:

$$\begin{aligned}
\frac{dA}{dt} &= \gamma \sqrt{\kappa} e^{\frac{(1-i\alpha_g)G(t-T) - (1-i\alpha_q)Q(t-T)}{2} + i\nu T} A(t-T) \\
&\quad - \gamma A + \gamma \mathcal{E}_i(t), \\
\frac{dG}{dt} &= g_0 - \gamma_g G - e^{-Q} (e^G - 1) |A|^2, \\
\frac{dQ}{dt} &= \gamma_q (q_0 - Q) - s (1 - e^{-Q}) |A|^2.
\end{aligned} \tag{1}$$

Here α_g and α_q are the linewidth enhancement factors in the gain and absorber sections, respectively, the delay parameter T stands for the cold cavity round-trip time, γ is the spectral filtering bandwidth, κ is the attenuation factor describing linear non-resonant intensity losses per cavity round trip, and s is the ratio of the saturation intensities in the gain and absorber

sections. The pump parameter g_0 depends on the injection current in the gain region, q_0 is the unsaturated absorption parameter, γ_g and γ_q are the carrier relaxation rates in the amplifying and absorbing sections, respectively. The parameter ν describes an additional detuning between the central frequency of the spectral filter and the closest cavity mode. The time variable t is normalized to the cold cavity round trip time, so that the delay parameter in the field equation is equal to unity, $T = 1$.

Let us assume that for vanishing injection amplitude, $\mathcal{E}_i(t) = 0$, the model equations (1) have a linearly-stable fundamental mode-locked solution

$$A(t) = A_0(t)e^{i\Omega t}, \quad G(t) = G_0(t), \quad Q(t) = Q_0(t),$$

where A_0 , G_0 , and Q_0 are time-periodic functions with the period T_0 close to the cavity round trip time T , $f_0 = 1/T_0$ is a corresponding repetition frequency, Ω is the detuning between the reference frequency and the closest spectral line of the unperturbed mode-locked comb, $|\Omega| \leq \pi f_0$.

In a laser with dual mode injection, injected frequencies are close to a certain optical spectral line of the free-running PML laser. Therefore, along this paper we assume that the optically injected field $\mathcal{E}_i(t)$ is given by

$$\mathcal{E}_i(t) = a e^{i[\Omega + \pi(2k+n)f_0]t} \cos(\pi n f t) e^{i2\pi\delta_\omega t}, \quad (2)$$

where a is the injection amplitude, integers k and $k + n$ are the numbers of two laser modes with the frequencies close to the injected tones, $n f$ is the frequency separation of the injected tones, $\delta_f = f - f_0 \ll f_0$ describes small detuning between the frequency f and the pulse repetition frequency of the uninjected laser, and δ_ω is an additional small shift of the two injected frequencies. It is noteworthy, that the experimental setup discussed later in Section 3 allows to access both the detuning parameters, δ_f and δ_ω .

Below we study theoretically the effect of dual-mode injection (2) on a PML laser with optical spectrum symmetric or almost symmetric with respect to some reference frequency. For example, for $\nu = \pi$ and $\alpha_{g,q} = 0$ in the model equations (1) the reference frequency coincides with the central frequency of the spectral filtering element and is located exactly in the middle between two adjacent longitudinal cavity modes of the PML laser, i.e. $\Omega = -\pi f_0$. Assuming that at zero detunings the injection is also symmetric, $2k + n = 1$, we rewrite expression (2) in the form:

$$\mathcal{E}_i(t) = a \cos(\pi n f t) e^{i2\pi\delta_\omega t}, \quad n = 1, 3, 5, \dots \quad (3)$$

2.1 Numerical calculation of the locking regions

In this section we present the results of numerical calculation of the boundaries of the domains in the parameter space where the laser pulse repetition frequency of the PML laser is locked to the external frequency f entering Eq. (2).

We consider a specific case of $\nu = \pi$ and symmetric or almost symmetric dual mode injection with the frequencies $\Omega - \pi n f_0$ and $\Omega + \pi n f_0$, where $n = 1$ and $n = 3$. Typical calculated optical spectra of the PML laser together with the indication of the frequencies of the optical injection are shown in Fig. 1.

To calculate the locking regions of a PML laser with dual frequency injection we used the same numerical procedure as in our previous studies of hybrid ML lasers [16]. First, to determine the

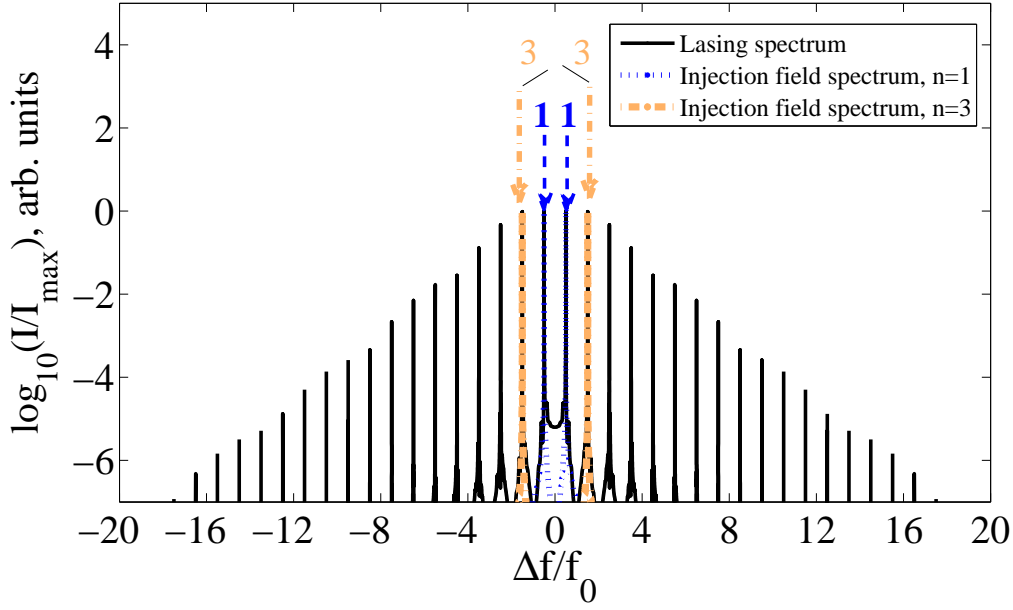


Figure 1: Spectrum of the free-running PML semiconductor laser (black solid line) for $\alpha_g = \alpha_q = 0$. Dashed (dashed-dotted) lines indicate the injection spectrum with $n = 1$ ($n = 3$) in Eq. (3).

pulse repetition frequency of the free running PML laser, we integrated the model equations (1) numerically with the parameter values given in Table 1 and zero external injection amplitude, $a = 0$. Next, to calculate the RF locking range for each consequent value of the RF detuning δ_f from an interval around $\delta_f = 0$ we performed numerical integration of the model equations (with the injection term (3) and $\delta_\omega = 0$) over the time-interval $2800T$ taking the solution calculated at the previous value of detuning δ_f as an initial condition. The boundaries of the RF locking range were determined by changing the RF detuning δ_f for vanishing optical frequency detuning, $\delta_\omega = 0$. Similarly, the boundaries of the optical frequency locking range were calculated by changing the value of optical frequency detuning δ_ω for vanishing RF detuning, $\delta_f = 0$. The results of these simulations for $n = 1$ are shown in Fig. 2 where local maxima of the field intensity time-trace $|A(t)|^2$ are plotted against δ_ω .

When the frequencies of the injected field come close enough to some modes in the mode-locking comb (see Fig. 1), these modes become locked to the external injection and the pulse repetition rate becomes equal to f . In the case of the injection into two adjacent modes, $n = 1$, the intensity of the resulting mode-locked regime is strictly periodic with the period $1/f$ and all the recorded intensity maxima have the same value at fixed detuning δ_ω (or δ_f). For frequency detuning outside the locking interval we have observed regimes with irregular or quasi-periodic pulsed laser intensity, which correspond to multiple intensity maxima at fixed detuning δ_ω (or δ_f) and, hence, a cloud of points in Fig. 2.

By estimating the locking range at different values of the injection field amplitude a we can obtain the locking regions (Arnold tongues) in the space of three parameters: RF and optical frequency detuning, δ_f and δ_ω , and the injected field amplitude a . The boundaries of the two-dimensional RF locking region calculated for vanishing optical frequency detuning $\delta_\omega = 0$ are shown in Fig. 3(a). Similarly, an optical frequency locking region calculated for vanishing RF detuning $\delta_f = 0$ is presented in Fig. 3(b). It can be seen from Fig. 3 that both the locking

Table 1: Typical parameter values used in simulations

spectral filtering bandwidth	γ	37.5
non-resonant field intensity attenuation factor per cavity round-trip	κ	0.3
linewidth enhancement factor in the gain section	α_g	0, 2
linewidth enhancement factor in the SA	α_q	0, 1
pump parameter	g_0	1.25
unsaturated absorption	q_0	5
gain relaxation rate	γ_g	0.025
SA relaxation rate	γ_q	2.5
ratio of gain/absorber saturation intensities	s	10
cold cavity round trip time	T	1
detuning	ν	π/T

ranges grow almost linearly with the injection field amplitude a . Furthermore, our simulations demonstrate that the optical frequency locking range shown in Fig. 3(b) is about ten times wider than the RF locking range in Fig. 3(a). Solid curves in Fig. 3 correspond to the case of zero linewidth enhancement factors, $\alpha_g = \alpha_q = 0$, while the dashed curves – to the case when $\alpha_g = 2$ and $\alpha_q = 1$. One can see from this figure that in the case of vanishing α -factors both optical and RF locking ranges are symmetric with respect to the zero frequency detuning. On the contrary, in the case of non-vanishing α -factors (dashed lines) locking ranges are asymmetric and shifted to the larger values of frequency detuning. This asymmetry is related to the increase of the pulse repetition frequency of free-running PML laser with the injection amplitude a and spectral shift of laser modes due to the non-vanishing α -factors. Similar asymmetry was observed experimentally in a quantum-dot PML laser (see next section). Furthermore, it can be seen from Fig. 3 that while the RF locking range has approximately the same width for zero and nonzero α -factors, the optical locking range is larger in the case of non vanishing α -factors.

Apart from a PML laser with dual-tone injection into a pair of adjacent modes ($n = 1$) we have considered the case of the optical injection into a pair of modes with the optical frequency separation close to $3 \cdot 2\pi f_0$ (i.e., $k = -1$ and $n = 3$ in Eq. (2)). The spectrum of the free-running PML and the two injected frequencies (dashed dotted lines) for this case are also presented in Fig. 1. The boundaries of the RF locking region calculated for vanishing optical frequency detuning $\delta_\omega = 0$ and the boundaries of the optical locking domain obtained for vanishing RF detuning $\delta_f = 0$ are shown in Fig. 4(a) and Fig. 4(b) respectively. Other parameters are as in Fig. 3. One can see from these figures that both RF and optical locking ranges have approximately the same width in the case of vanishing α -factors (black curves in Fig. 4(a) and Fig. 4(b).) Furthermore, since the injected frequencies are symmetric with respect to the zero frequency detuning point both locking tongues are also symmetric with respect to this point. It follows from Fig. 4 that RF locking range in the case of non-vanishing α -factors is approximately ten times smaller than optical locking range, see dashed curves in Fig. 4(a) and Fig. 4(b). As it can be seen from Fig. 3, similarly to the case with $n = 1$ both locking ranges are asymmetric with respect to the zero frequency detuning. Comparing Fig. 3 and Fig. 4 one can conclude that RF and optical locking ranges have approximately the same width for the cases when the frequency separation between the two injected frequencies is close to $2\pi f_0$ or $3 \cdot 2\pi f_0$ and α -factors are not zero.

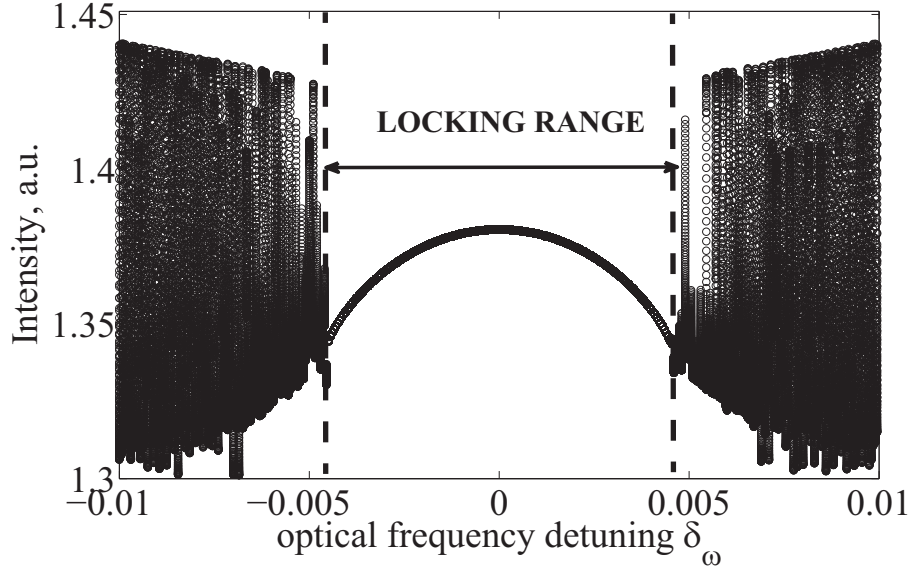


Figure 2: Numerical estimation of the optical locking range of passively ML semiconductor laser with dual mode optical injection. Local maxima of the intensity timetrace and at a fixed injection field amplitude $a = 0.008$. On the x axis is optical frequency detuning δ_ω . RF detuning $\delta_f = 0$.

A similar situation was encountered in our study of hybrid mode-locked lasers, see Ref. [16]. It was demonstrated in this study that the locking range has approximately the same width when the reverse bias applied to the laser absorber section is modulated with a frequency close to f_0 and with a frequency approximately twice larger than f_0 .

3 Experiment

The experimental study of the locking combs was done for a quantum dot PML laser with a 10 GHz repetition rate. For the dual-tone injection, the light from the Agilent tunable laser source was modulated by a Mach-Zehnder amplitude modulator driven via an amplified Rohde&Schwarz SMR 60 signal generator to produce coherent tones. The diagram of the experimental setup is shown in Fig. 5. For the injection into two adjacent laser modes, the driver frequency was set close to half the repetition rate of the slave laser, giving sidebands separation close to the fundamental frequency of mode-locking, f_{rep} .

Injection-locking to a dual-tone source requires that both injected optical frequencies are close to the respective longitudinal modes of the uninjected PML laser, and that the beating frequency between the injected modes lies within a narrow locking range around the repetition rate of the uninjected laser. Due to injection induced carrier density change leading to the refractive index decrease the repetition rate of the injected laser was up-shifted from that of the uninjected laser. The shift ranged from a few 10s up to 100s of MHz, depending on the device and bias conditions. Stable operation was achieved over a range of ± 10 MHz around the injected laser repetition rate. The measured evolution of the injected mode-locked laser RF spectrum versus modulator frequency, f_{mod} , is shown in Fig. 6 (a). When the PML laser was locked to the dual-tone injection, its timing jitter and RF linewidth reduced greatly and the pulse repetition rate followed the injection tones frequency separation, F_2 .

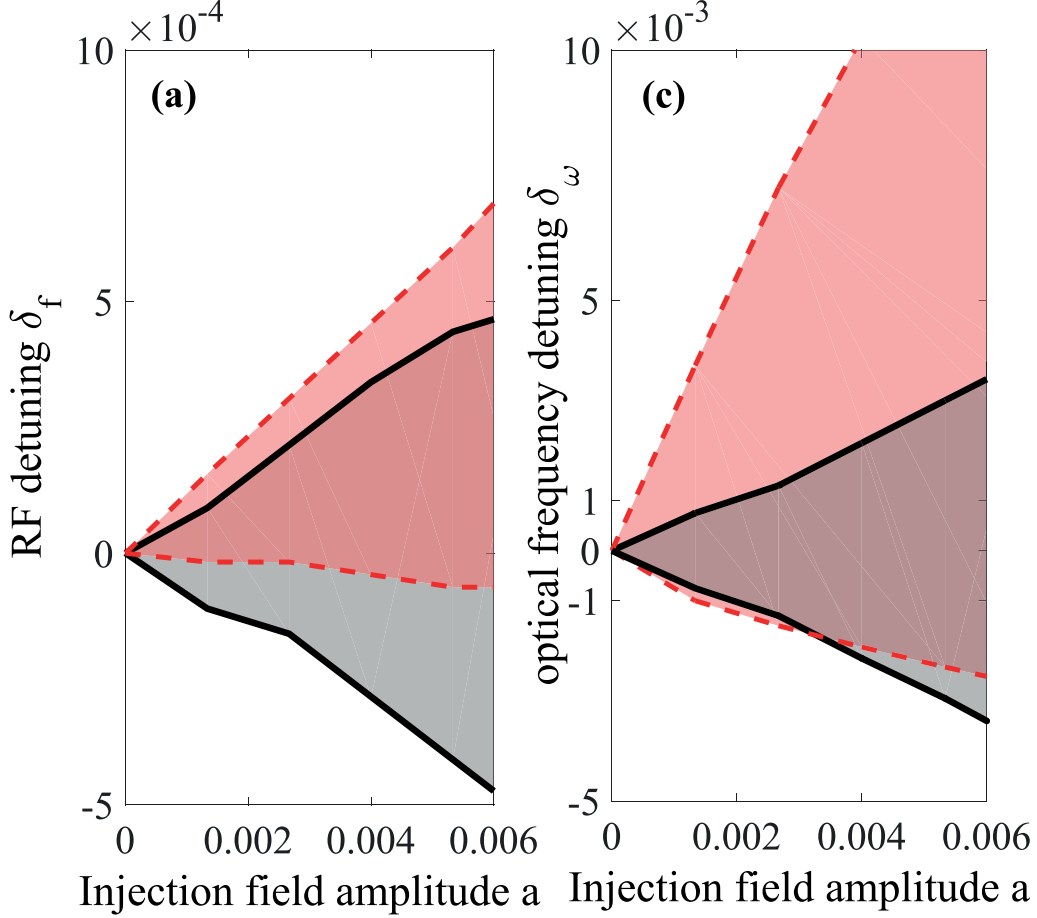


Figure 3: RF locking region at $\delta_\omega = 0$ (a) and optical frequency locking region at $\delta_f = 0$ (b). Frequency separation of the injected tones is close to the laser free spectral range, $n = 1$. Solid black (dashed red) curves mark the boundaries of the correspondingly shaded locking regions for $\alpha_g = \alpha_q = 0$ ($\alpha_g = 2, \alpha_q = 1$).

Fig. 6 (b) shows the RF locking range versus the injection power. The optical frequency of the tunable laser was chosen optimal to achieve the largest RF locking range in these measurements and kept constant with the injection power. Dual-tone injection-locking allowed tuning of the injected laser pulse repetition rate over a 25 MHz.

For the optical locking range measurements the tones separation F_2 was chosen in the middle of the RF locking range, so that the RF detuning was close to zero, and the central wavelength of the injection was varied. The evolution of optical and electronic spectra with the central wavelength detuning are shown in Fig. 7 (a) and (b), respectively. When the PML laser was locked to both the injected frequencies, its optical spectrum was narrowed, the repetition rate up-shifted, as discussed above, and the RF noise reduced greatly. The optical frequency locking combs for the case of the injection into two adjacent modes are shown in Fig. 8. The locking ranges were measured in two parameter space: injection power δ and frequency detuning. The optical locking range was much wider than the RF locking range discussed above and reached the values of a few GHz.

To achieve higher frequency separations between the injected sidebands, we set the signal generator at ~ 15 GHz, which corresponds to $F_2 \sim 3 * f_{rep}$ (see dashed-dotted lines in Fig.1). Similarly to the injection of adjacent modes, dual-tone injection into a pair of third-neighbor

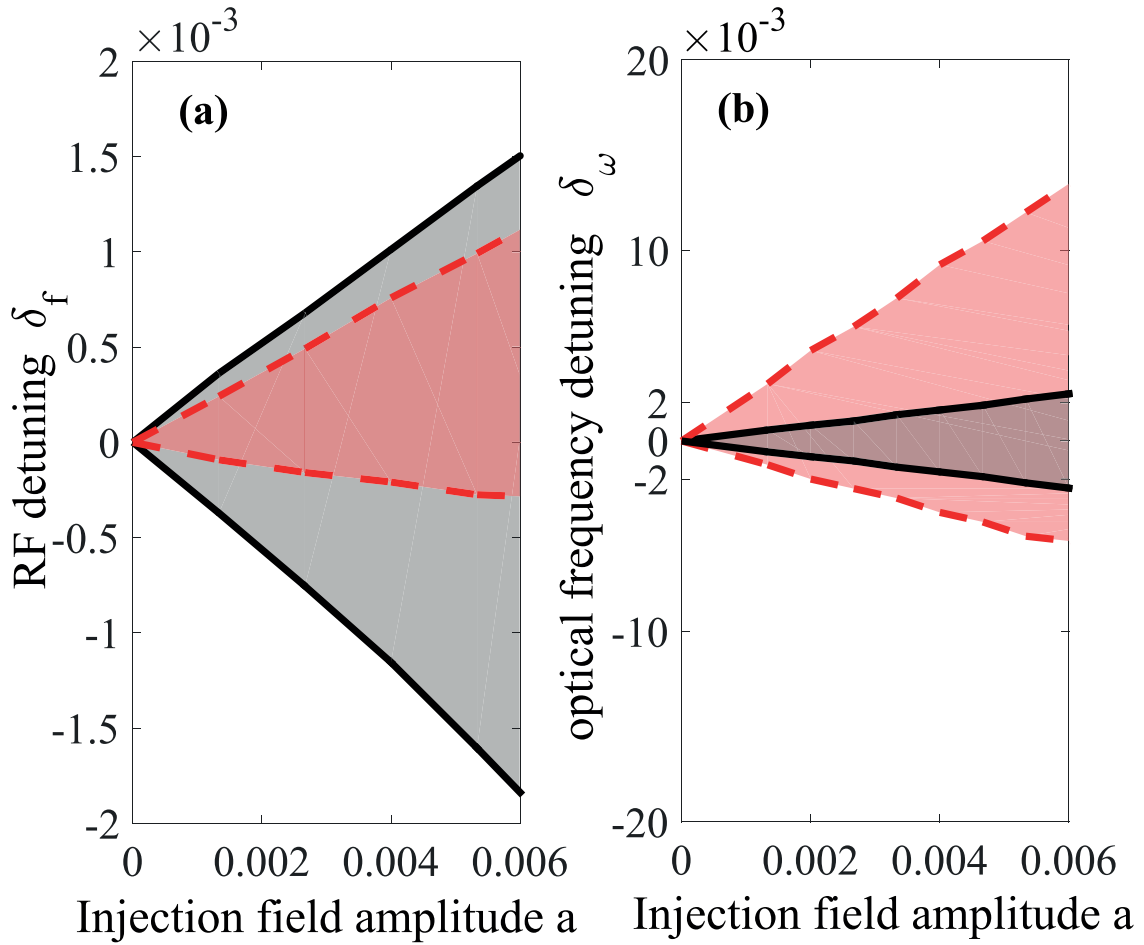


Figure 4: RF locking region at $\delta_\omega = 0$ (a) and optical frequency locking region at $\delta_f = 0$ (b) in a laser with two external frequencies injected into a pair of third-neighbor modes, $n = 3$. Solid black (dashed red) curves mark the boundaries of the correspondingly shaded locking regions for $\alpha_g = \alpha_q = 0$ ($\alpha_g = 2, \alpha_q = 1$). Other parameters are as in Fig. 3.

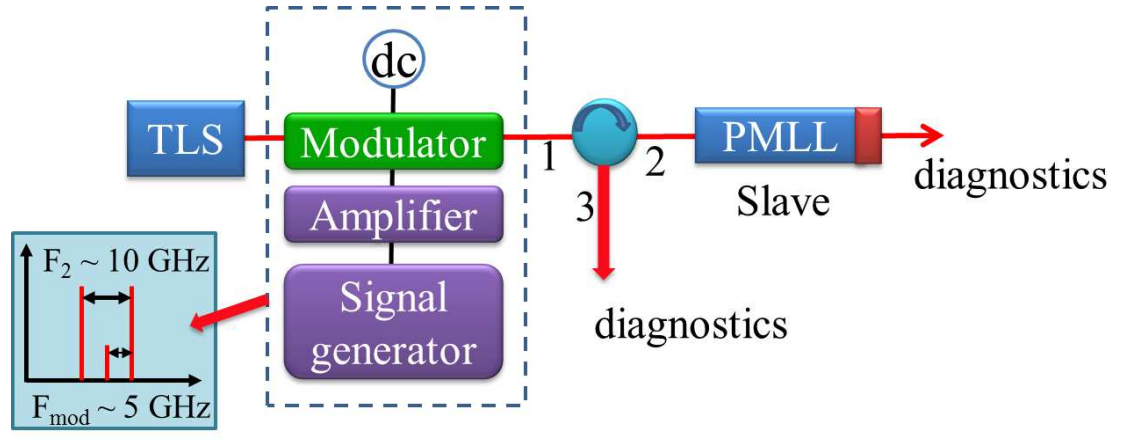


Figure 5: Experimental setup for dual-tone coherent injection into a PML laser (PMLL). Inset shows schematic diagram of the modulator optical spectrum with the suppressed carrier frequency.

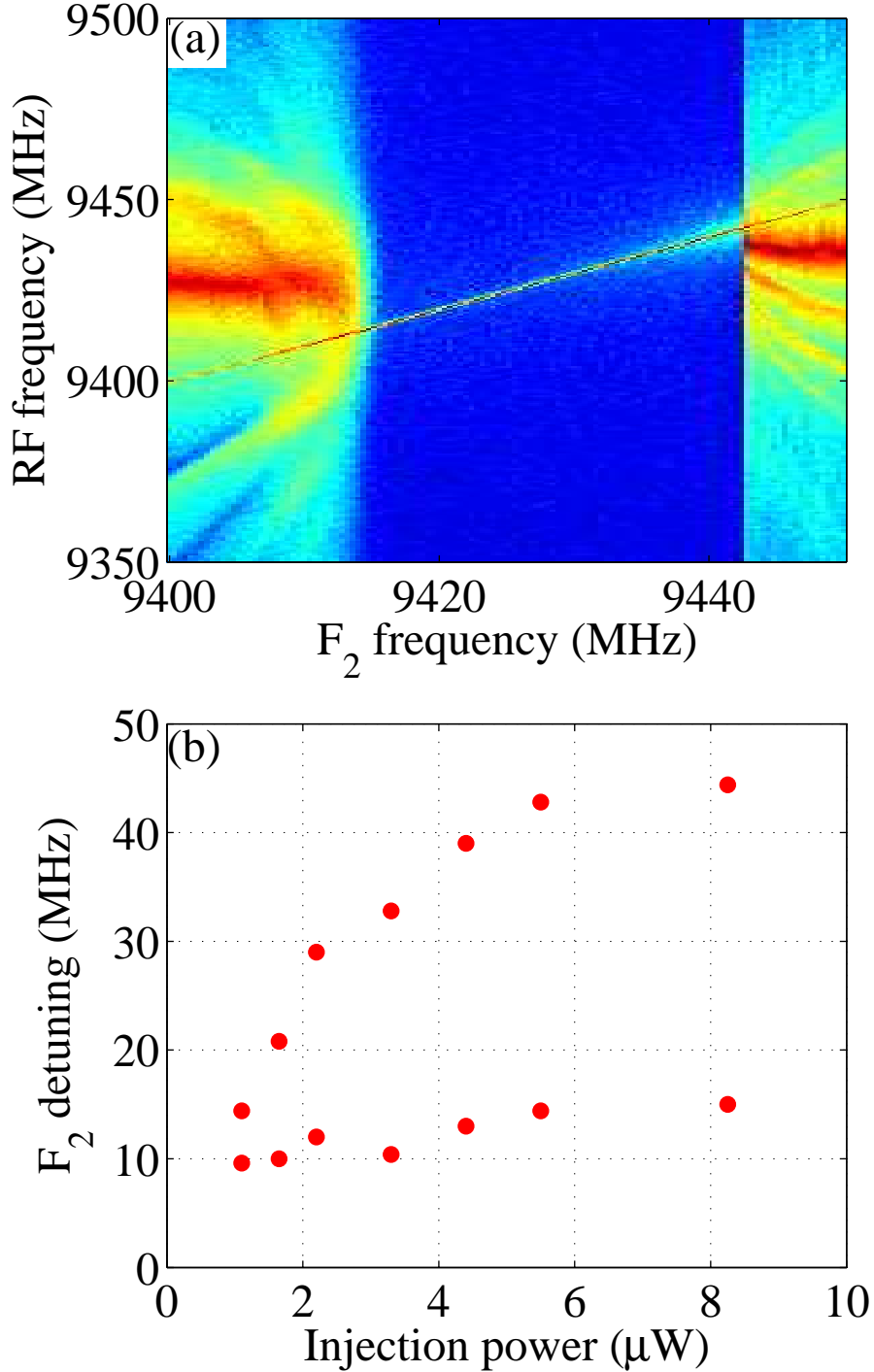


Figure 6: (a) Evolution of the PML laser RF spectrum with frequency separation of two injected tones. (b) Red dots indicate boundaries of the locking region on the plane of two parameters: RF modulation frequency and injection power. Gain current: 100 mA; absorber bias: -6.0 V.

modes allowed timing jitter reduction, RF linewidth and modal optical linewidth, as well as optical spectrum narrowing [17]. Fig. 9 shows the measured evolution of the injected laser RF spectrum versus modulation frequency change for the $F_2 \sim 3 * f_{rep}$. We scaled the abscissa to $F_2/3$ in order to show an RF locking range more clearly. When the laser was locked to the injected tones, its repetition rate followed the fraction of the master tones frequency separation, $F_2/3$, for ~ 17

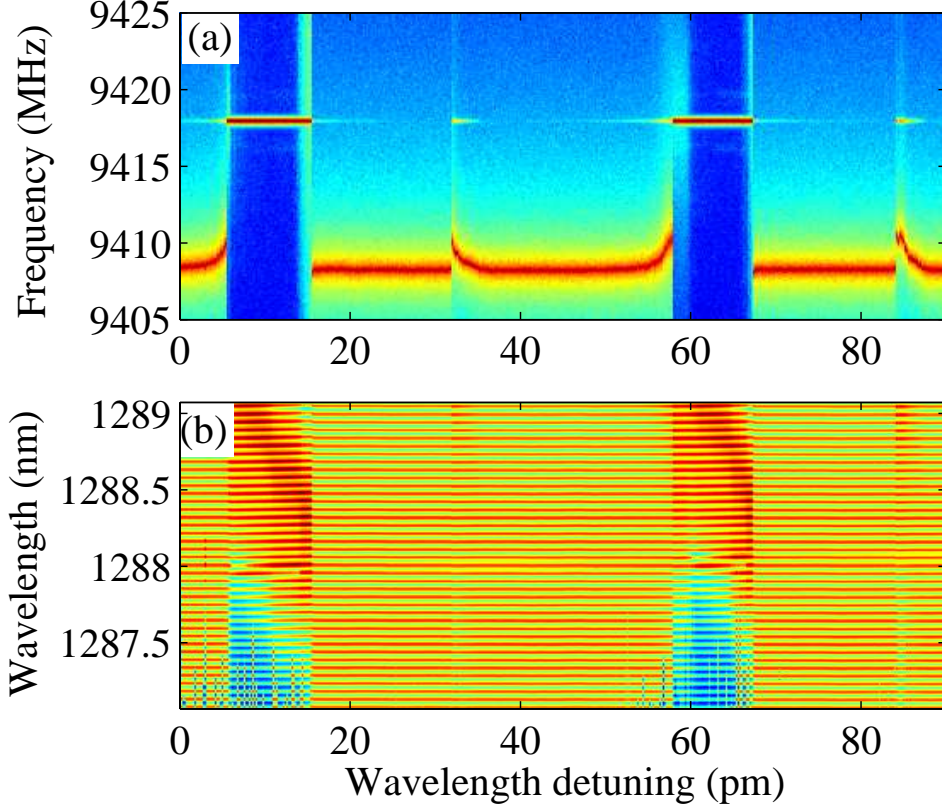


Figure 7: (a) Evolution of the laser RF spectrum (a) and optical spectrum (b) with the injection wavelength detuning. Gain current: 100 mA; absorber bias: -6.0 V.

MHz. Remarkably, the RF locking range was not significantly different from that obtained for the smaller tone separation (see Fig.6). Similar outcome was achieved theoretically for non-zero α -factors (see Fig.3 and see Fig.4).

4 Asymptotic analysis

In this section using an approach similar to that described in Ref. [28] we derive asymptotic formula for RF and optical locking ranges. For simplicity of our analysis we consider the case when the center of the spectral filtering profile is located exactly in the middle between two cavity modes, $\nu T = \pi$ in a laser with vanishing α -factors, $\alpha_{g,q} = 0$, and assume a “symmetric” optical injection (3). Since in this case $e^{i\nu T} = -1$, all the coefficients of the unperturbed system Eqs. (1) with $a = 0$ are real, this system possesses a mode-locked solution with real amplitude $A = A_0(t)$ and T_0 -periodic intensity $|A_0(t + T_0)|^2 = |A_0(t)|^2$. However, instead of being T_0 -periodic, the amplitude A_0 is only $2T_0$ -periodic in time. This is related to the fact that due to the presence of the factor $e^{i\nu T} = -1$ in the right hand side of the first equation in (1) every next pulse has an inverted phase with respect to the previous one. Therefore, in the analysis below it is convenient to consider the periodic mode-locked solution of the unperturbed problem on the interval of the length $2T_0$. In the limit of small injection amplitude, $a \ll 1$, we look for a solution

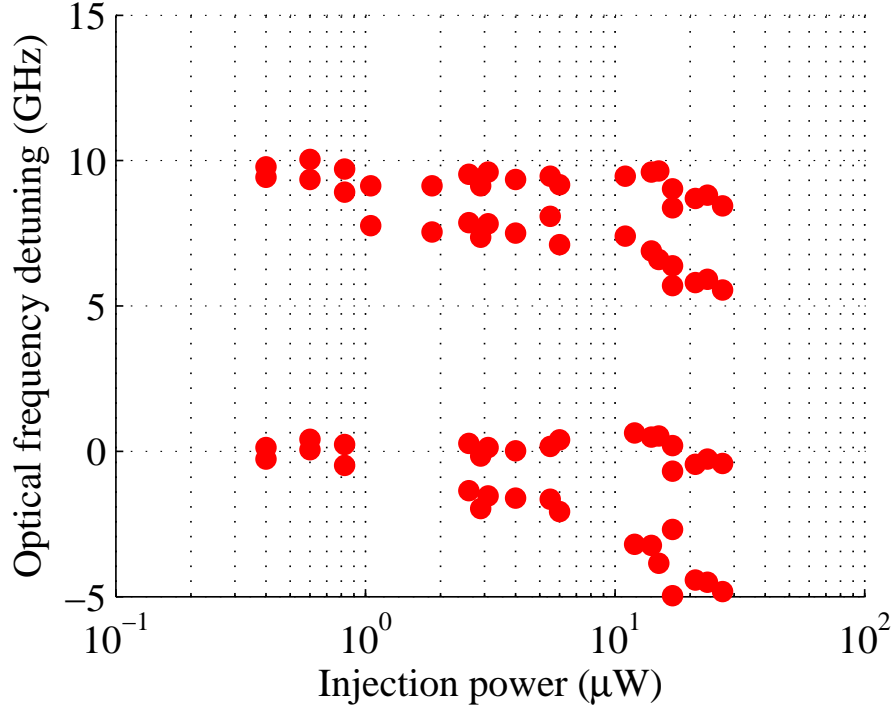


Figure 8: Optical frequency locking ranges for two adjacent modes versus injection power. Gain current: 100 mA; absorber bias: -6.0 V.

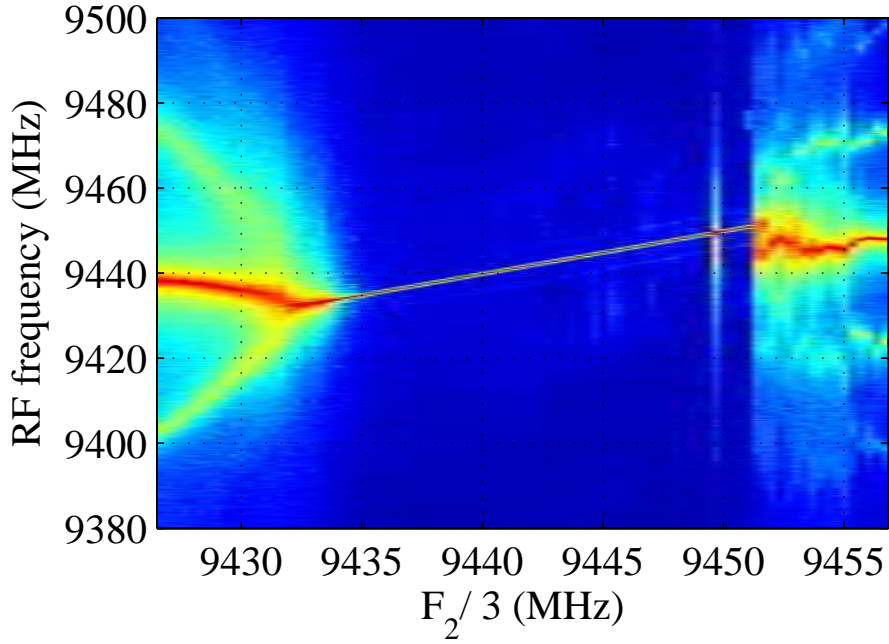


Figure 9: Evolution of the laser RF spectrum with sidebands separation frequency change. Gain current: 120 mA; absorber bias: -6.0 V.

of Eqs. (1) in the form

$$A = e^{i\varphi} [A_0(\tau_0 + \theta) + aA_1(\tau_0 + \theta, \tau_1) + \dots], \quad (4)$$

$$G = G_0(\tau_0 + \theta) + aG_1(\tau_0 + \theta, \tau_1) + \dots, \quad (5)$$

$$Q = Q_0(\tau_0 + \theta) + aQ_1(\tau_0 + \theta, \tau_1) + \dots, \quad (6)$$

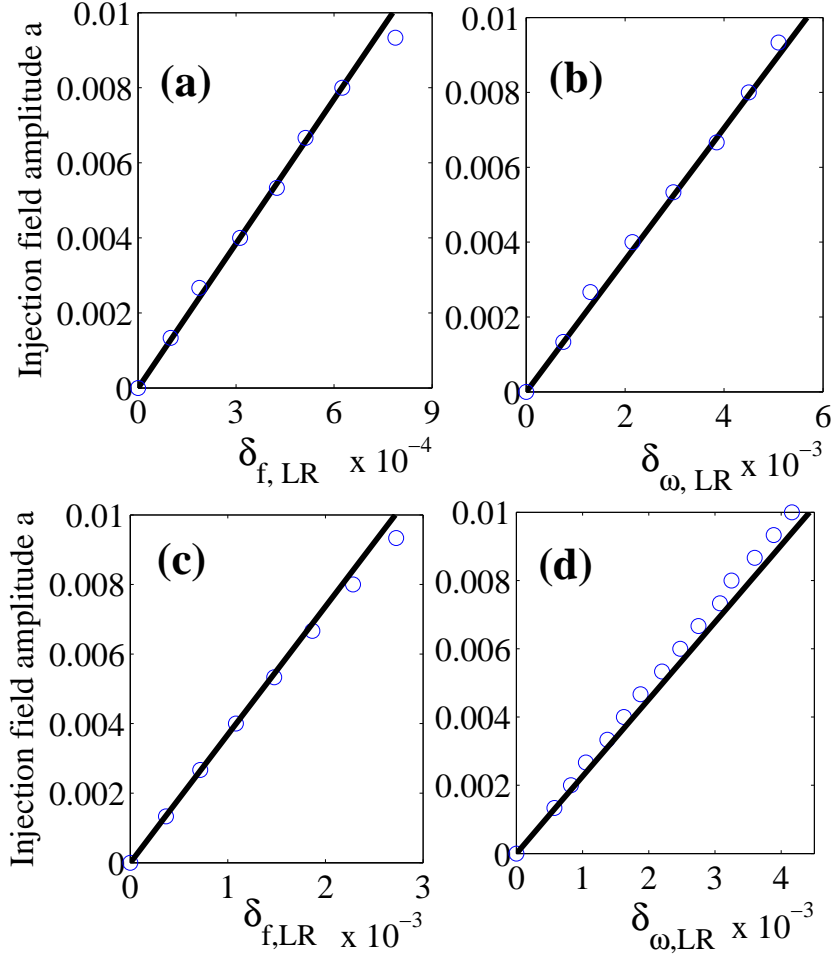


Figure 10: Estimation of the locking region in dependence on the injection field amplitude a when $n = 1$ (a)-(b) and $n = 3$ (c)-(d). Black solid line - results obtained by asymptotic analysis, dots - numerical simulations.

where φ and θ are functions of the “slow” time $\tau_1 = at$, $\tau_0 = t$ is the “fast” time, real functions $A_0(t)$, $G_0(t)$, and $Q_0(t)$ define a $2T_0$ -periodic mode-locked solution of the unperturbed Eqs. (1). Furthermore, we assume that the small frequency detuning parameters are of order a , $\delta_\omega = a\Delta_\omega$ and $\delta_f = a\Delta_f$. Substituting these expressions into (1) and collecting the first order terms in small parameter a we get the following linear system of DDEs for the 4-dimensional vector $\vec{\psi}_1 = (\text{Re } A_1, \text{Im } A_1, G_1, Q_1)^T$:

$$\hat{L}\vec{\psi}_1 = \vec{P}(t)\frac{d\theta}{d\tau_1} + \vec{S}(t)\frac{d\varphi}{d\tau_1} - \vec{R}, \quad (7)$$

where the vectors $\vec{P}(t)$ and $\vec{S}(t)$ are given by:

$$\vec{P} = \vec{\chi}_\theta + T\frac{d^2\vec{\psi}_0}{dt^2} + \gamma T\frac{d\vec{\psi}_0}{dt}, \quad (8)$$

$$\vec{S} = \vec{\chi}_\varphi(1 + \gamma T) + T\frac{d\vec{\chi}_\varphi}{dt} \quad (9)$$

with $\vec{\psi}_0 = (A_0, 0, 0, 0)^T$, and the linear operator \hat{L} is defined by

$$\hat{L}\vec{\psi} = -\frac{\partial\vec{\psi}}{\partial t} + B(t)\vec{\psi} + C(t-T)\vec{\psi}(t-T), \quad (10)$$

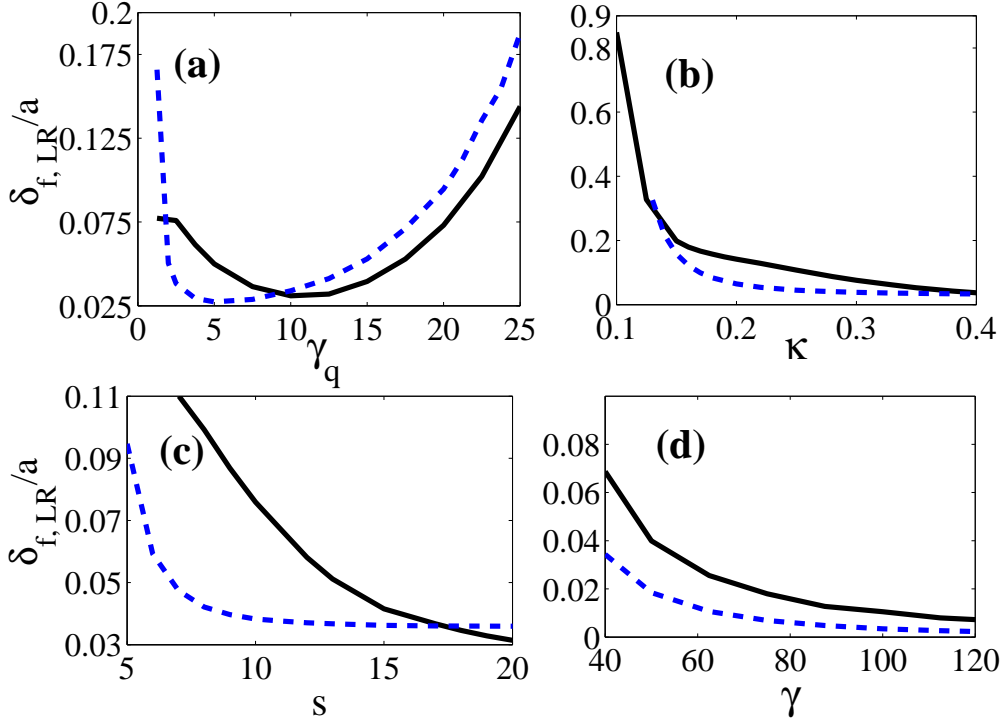


Figure 11: Dependence of $\delta_{f,LR}/a$ on the model parameters. Black solid and dashed lines correspond to $g_0 = 1.25, g_0 = 2$ respectively. Other parameter values are as in Table 1.

with $2T_0$ -periodic matrices B and C given in Appendix. The neutral modes

$$\vec{\chi}_\theta = \frac{d}{dt}(A_0, 0, G_0, Q_0)^T,$$

$$\vec{\chi}_\varphi = (0, -A_0, 0, 0)^T,$$

entering Eqs. (8) and (9) correspond to time and phase shift symmetries of Eqs. (1). Here T denotes transposition. The neutral modes are eigenfunctions of the operator \hat{L} corresponding to zero eigenvalues, $\hat{L}\vec{\chi}_{\theta,\varphi} = 0$. Using (3) and neglecting second order terms in a we get the following expression for the quantity \vec{R} in the right hand side of (7):

$$\vec{R} = \gamma \cos \nu (\cos \mu, \sin \mu, 0, 0)^T$$

with $\nu = n\pi f_0(\tau_0 - \theta) + n\pi\Delta_f\tau_1$ and $\mu = 2\pi\Delta_\omega\tau_1 - \varphi$.

According to the Fredholm alternative solvability of Eq. (7) requires the orthogonality of its right hand side to the solutions $\vec{\chi}_{\theta,\varphi}^\dagger$ of the equation adjoint to the equation $\hat{L}\vec{\psi} = 0$. This equation reads

$$\hat{L}^\dagger\vec{\psi}^\dagger = \frac{\partial\vec{\psi}^\dagger}{\partial t} + B^T(t)\vec{\psi}^\dagger + C^T(t)\vec{\psi}^\dagger(t+T) = 0. \quad (11)$$

Hence, using the biorthogonality property of the vectors $\vec{\chi}$ and $\vec{\chi}^\dagger$ we rewrite solvability condition

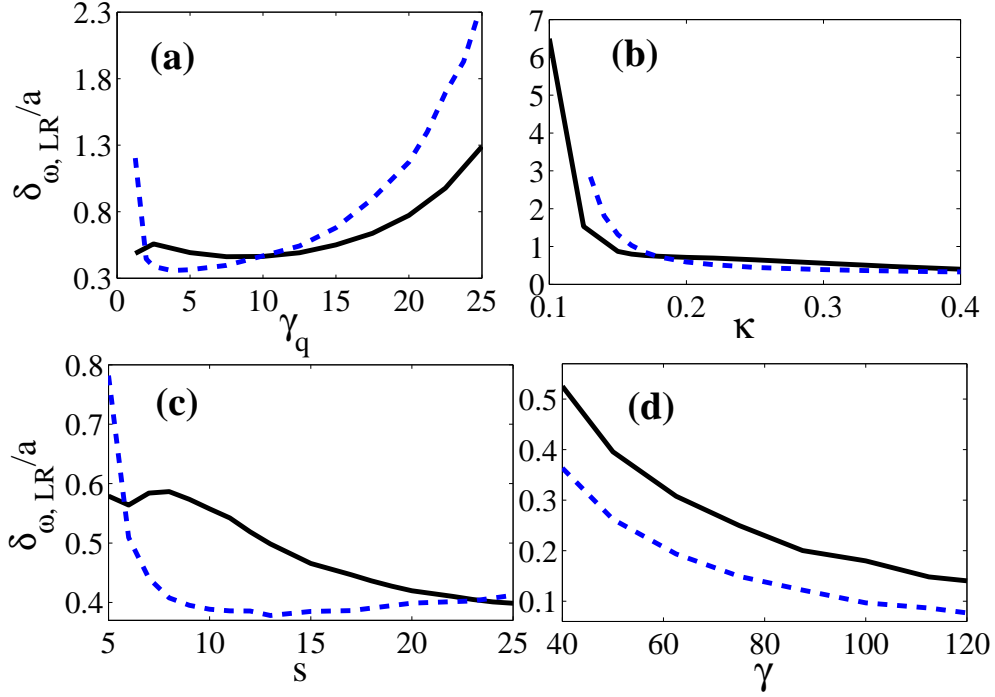


Figure 12: Dependence of $\delta_{\omega, LR}/a$ on the model parameters. Black solid and dashed lines correspond to $g_0 = 1.25, g_0 = 2$ respectively. Other parameter values are as in Table 1.

as a set of two differential equations governing slow time evolution of two phases, θ and φ :

$$\frac{d\theta}{d\tau_1} = c_\theta^{-1} \int_0^{2T_0} \chi_{\theta 1}^\dagger \cos \nu \cos \mu d\tau_0, \quad (12)$$

$$\frac{d\varphi}{d\tau_1} = c_\varphi^{-1} \int_0^{2T_0} \chi_{\varphi 2}^\dagger \cos \nu \sin \mu d\tau_0, \quad (13)$$

where the expressions for the coefficients c_θ and c_φ are given in the Appendix. $\chi_{\theta 1}^\dagger$ and $\chi_{\varphi 2}^\dagger$ are the components of the vectors $\vec{\chi}_\theta^\dagger(\tau_0) = (\chi_{\theta 1}^\dagger, 0, \chi_{\theta 3}^\dagger, \chi_{\theta 4}^\dagger)$ and $\vec{\chi}_\varphi^\dagger(\tau_0) = (0, \chi_{\varphi 2}^\dagger, 0, 0, 0)$, respectively, which are the eigenmodes of \hat{L}^\dagger defined by (11). For more details see Refs. [16,28]. After the coordinate change $\theta = (\Theta + \Delta_f \tau_1)/f_0$ and $\varphi = \Phi + 2\pi \Delta_\omega \tau_1$ the system (12) and (13) takes the form

$$\frac{d\Theta}{d\tau_1} = -\Delta_f + f_0 d_\theta^{(n)} \cos(\Phi) \cos(n\pi\Theta + \xi_\theta^{(n)}), \quad (14)$$

$$\frac{d\Phi}{d\tau_1} = -2\pi \Delta_\omega - d_\varphi^{(n)} \sin(\Phi) \cos(n\pi\Theta + \xi_\varphi^{(n)}). \quad (15)$$

Expressions of the complex coefficients $d_{\theta, \varphi}^{(n)}$ and $\xi_{\theta, \varphi}^{(n)}$ with the index n describing the separation of the injected modes are given in Appendix. From (14) and (15) we get the width of the optical and RF locking ranges:

$$\delta_{\omega, LR} = \frac{a}{2\pi} |d_\varphi^{(n)}| \quad \text{and} \quad \delta_{f, LR} = \frac{a}{T_0} |d_\theta^{(n)}|. \quad (16)$$

In Fig. 10 the half-width of the optical and RF locking ranges (16) are compared to those calculated by direct numerical integration of Eq. (1) with $\alpha_{g, q} = 0$ and an optical injection given

by Eq. (3) with $n = 1$ (Fig. 10a,b) and $n = 3$ (Fig. 10a,b). One can see that the asymptotic relations (16) give a good approximation of the width of the locking range even for relatively large injected field amplitudes a . Our numerical simulations and asymptotic analysis indicate that optical-frequency locking range is about 10 times larger than RF locking range in the case of the injection into a pair of adjacent modes (see Fig. 10). On the contrary, the widths of two locking ranges become comparable for the dual-mode injection into a pair of third-neighbor modes (see Fig. 1).

Asymptotic widths of the locking range characterize the ability of the PML regime to be locked to the dual mode injection. The dependence of the optical and RF locking range widths on the parameters of Eq. (1) is illustrated in Figs. 11 and 12, respectively. In particular, Figs. 11a and 12a show the dependence of the locking range width on the absorber relaxation rate γ_q . Experimentally it was demonstrated that the locking range increases with the absolute value of the voltage applied to the absorber section [22]. On the other hand, it is known that the absorber relaxation rate γ_q increases with the absolute value of the reverse voltage applied to the absorber section. It can be seen from Figs. 11 and 12 that both the RF locking range and optical frequency locking range have parabolic dependence on γ_q .

Our simulations indicate that the RF locking range is ten times smaller than the optical locking range. It can be easily seen that the widths of the locking ranges decrease with the increase of the parameters κ , s , and γ . A similar dependence of the locking range width on the model parameters was observed in our study of hybrid mode-locking in semiconductor lasers in [16]. Finally, we note that similar asymptotic approach can be used to study the effect of noise on pulse timing jitter and modal line width in a PML laser under the dual mode coherent optical injection, which will be the subject of the future works. Asymptotic approach for pulse timing jitter estimation in PML lasers with and without delayed optical feedback was developed in [29, 30].

5 Conclusion

We have performed theoretical and experimental study of the locking characteristics of a PML laser under the dual mode coherent optical injection. It has been demonstrated numerically that the widths of the RF and optical locking ranges increase almost linearly with the injection field amplitude. In the case of non-zero α -factors both the RF and optical locking ranges are asymmetric with respect to the pulse repetition frequency of the free-running PML laser. This asymmetry is related to the increase of the pulse repetition rate with the injection amplitude.

Our numerical simulations indicate that the optical locking range is ~ 10 -30 times larger than the RF locking range for $n = 1$. We have also demonstrated numerically that the optical locking range can be one order of magnitude larger than the RF locking range when the frequency separation between two injected modes is close to the 3rd harmonic of the free-running PML laser repetition frequency. The values of the locking ranges calculated in this case for non-zero α -factors had similar values when compared to the injection locking of two adjacent modes.

The RF and optical locking ranges were measured in a 10-GHz quantum dot PML laser versus the injection power. In qualitative agreement with the theoretical results, the measured optical locking range was much wider than the RF locking range. Experiments demonstrated the optical locking ranges widths reaching a few GHz and the RF tuning in the tens of MHz range. This is in qualitative agreement with our theoretical results obtained in the case of non-zero α -factors.

Analytical estimates of the locking range width have been obtained using an asymptotic ap-

proach in the limit of small injection amplitude. According to these estimates the width of the optical and RF locking ranges has parabolic dependence on the absorber relaxation rate γ_q and decreases with the decrease of the parameters γ , s , and κ , which describe the spectral filtering bandwidth, the ratio of the saturation intensities in the gain and absorber sections, and linear attenuation per cavity round trip, respectively. Similar dependence of the locking range width on the parameters of the model equations was observed in our previous study of hybrid mode-locked lasers [16].

Appendix

The matrices $B(t)$ and $C(t)$ in (10) are defined by the relations

$$B = \begin{pmatrix} -\gamma & 0 & 0 & 0 \\ 0 & -\gamma & 0 & 0 \\ -hA_0 & 0 & -\gamma_g - e^{G_0 - Q_0}|A_0|^2 & \frac{h}{2}|A_0|^2 \\ -pA_0 & 0 & 0 & -\gamma_q - se^{-Q_0}|A_0|^2 \end{pmatrix},$$

with $h = 2e^{-Q_0}(e^{G_0} - 1)$ and $p = 2s(1 - e^{-Q_0})$,

$$C = \gamma\sqrt{\kappa}e^{\frac{G_0 - Q_0}{2}} \begin{pmatrix} 1 & 0 & \frac{1}{2}A_0 & -\frac{1}{2}A_0 \\ 0 & 1 & 0 & 0 \\ 0 & 0 & 0 & 0 \\ 0 & 0 & 0 & 0 \end{pmatrix},$$

$$c_\theta = \gamma^{-1} \left(1 + T \int_0^{2T_0} \frac{d}{dt} \left(\gamma A_0 + \frac{dA_0}{dt} \right) \chi_{\theta 1}^\dagger dt \right),$$

$$c_\varphi = \gamma^{-1} \left(1 + \gamma T + T \int_0^{2T_0} \frac{dA_0}{dt} \chi_{\varphi 2}^\dagger dt \right),$$

where $\chi_{\theta 1}^\dagger$ and $\chi_{\varphi 1}^\dagger$ are the components of the neutral modes of the adjoint linear operator \hat{L}^\dagger defined by Eq. (11).

The coefficients $d_{\theta,\varphi}^{(n)}$ and $\xi_{\theta,\varphi}^{(n)}$ in Eqs. (14)-(15) are given by

$$d_{\theta,\varphi}^{(n)} = c_{\theta,\varphi}^{-1} |F_{\theta,\varphi}^{(n)}|, \quad \xi_{\theta,\varphi}^{(n)} = \arctan \frac{\text{Im } F_{\theta,\varphi}^{(n)}}{\text{Re } F_{\theta,\varphi}^{(n)}},$$

where $F_{\theta,\varphi}^{(n)}$ are the Fourier coefficients of $\chi_{\theta 1}^\dagger(t)$ and $\chi_{\varphi 2}^\dagger(t)$:

$$F_\theta^{(n)} = \int_0^{2T_0} \chi_{\theta 1}^\dagger(t) e^{-i\pi n f_0 t} dt,$$

$$F_\varphi^{(n)} = \int_0^{2T_0} \chi_{\varphi 2}^\dagger(t) e^{-i\pi n f_0 t} dt.$$

References

- [1] D. Bimberg, M. Grudmann, and N. N. Ledentsov, Quantum dot heterostructures. J. Wiley, 1999.
- [2] D. Bimberg, "Quantum dot based nanophotonics and nanoelectronics," Electron. Lett. **44**, pp. 168–171, 2008.
- [3] E. U. Rafailov, M. A. Cataluna, and E. Avrutin , Ultrafast Lasers Based on Quantum-dot Structures: Physics and Devices. WILEY-VCH Verlag, 2011.
- [4] P. J. Delfyett, S. Gee, M.-T. Choi, H. Izadpanah, W. Lee, S. Ozharar, F. Quinlan, and T. Yilmaz, "Optical frequency combs from semiconductor lasers and applications in ultrawide-band signal processing and communications," J. Lightwave Technol. **24**, pp. 2701–2719, 2006.
- [5] M. Costa e Silva, A. Lagrost, L. Bramerie, M. Gay, P. Besnard, M. Joindot, J. C. Simon, A. Shen, and G.H. Duan, in Optical Fiber Communication (OFC), collocated National Fiber Optic Engineers Conference, 2010 Conference on (OFC/NFOEC), Lannion, France, 21-25 March 2010, pp. 1–3.
- [6] M. G. Thompson, C. Marinelli, K. T. Tan, K. A. Williams, R. V. Penty, I. H. White, I. N. Kaiander, R. L. Sellin, D. Bimberg, D. J. Kang, M. G. Blamire, F. Visinka, S. Jochum, and S. Hansmann, Electron. Lett. **39**, p. 1121, 2003.
- [7] D. Bimberg, G. Fiol, M. Kuntz, C. Meuer, M. Lämmlin, N.N. Ledentsov, and A.R. Kovsh, "High speed nanophotonic devices based on quantum dots," Phys. Stat. Sol.(a) **203**, pp. 3523–3532, 2006.
- [8] M. Kuntz, G. Fiol, M. Laemmlin, C. Meuer, and D. Bimberg, "High speed mode-locked quantum dot lasers and optical amplifiers," Proceedings of the IEEE **95**, pp. 1767–1778, 2007.
- [9] D. Bimberg, "Quantum dots for lasers, amplifiers and computing," J. Phys. D **38**, pp. 2055–2058, 2005.
- [10] M. Kuntz G. Fiol, M. Lammlin, D. Bimberg, M.G. Thompson, K.T. Tan, C. Marinelli, A. Wonfor, R. Sellin, R.V. Penty, I.H. White, V.M. Ustinov, A.E. Zhukov, Y.M. Shernyakov, A.R. Kovsh, N.N. Ledentsov, C. Schubert, and V. Marembert, "Direct modulation and mode locking of 1.3 μm quantum dot lasers," New J. Phys. **6**, p. 181, 2004.
- [11] R. Kaiser and B. Hüttl, "Monolithic 40-GHz Mode-Locked MQW DBR Lasers for High-Speed Optical Communication Systems," IEEE J. Sel. Top. Quant. Electron. **13**, pp. 125–135, 2007.
- [12] M.G. Thompson, A.R. Rae, Mo Xia, R.V. Penty, and I.H. White, "InGaAs quantum dot mode-locked laser diodes," IEEE J. Sel. Top. Quant. Electron. **15**, pp. 661–672, 2009.
- [13] G. Fiol, D. Arsenijević, D. Bimberg, A. G. Vladimirov, M. Wolfrum, E. A. Viktorov, and P. Mandel, "Hybrid mode-locking in a 40 GHz monolithic quantum dot laser ," Appl. Phys. Lett **96**, p. 011104, 2010.

- [14] T. Habruseva, Shane O'Donoghue, N. Rebrova, D. A. Reid, Liam P. Barry, Stephen P. Hegarty, D. Rachinskii, and G. Huyet, "Quantum-Dot Mode-Locked Lasers with Dual Mode Optical Injection," IEEE Phot. Tech. Lett. **22(6)**, pp. 359–361, 2009.
- [15] H. Schmeckeber, G. Fiol, C. Meuer, D. Arsenijević, and D. Bimberg, "Complete pulse characterization of quantum-dot mode-locked lasers suitable for optical communications up to 160 Gbit/s," Opt. Express **18**, pp. 3415–3425, 2004.
- [16] R. Arkhipov, A. Pimenov, M. Radziunas, D. Rachinskii, A.G. Vladimirov, D. Arsenijevic, H. Schmeckeber, and D. Bimberg, "Hybrid Mode Locking in Semiconductor Lasers: Simulations, Analysis, and Experiments," IEEE J. Sel. Top. Quant. Electron. **19(6)**, p. 1100208, 2013.
- [17] T. Habruseva, G. Huyet and S. P. Hegarty, "Dynamics of Quantum-Dot Mode-Locked Lasers With Optical Injection," IEEE J. Sel. Top. Quant. Electron. **17(5)**, pp. 1272–1279, 2011.
- [18] T. Habruseva, S. P. Hegarty, A. G. Vladimirov, A. Pimenov, D. Rachinskii, E. A. Viktorov and G. Huyet, "Bistable regimes in an optically injected mode-locked laser," Optics Express **20(23)**, p. 25572, 2012.
- [19] A. Pimenov, E. A. Viktorov, S. P. Hegarty, T. Habruseva, G. Huyet, D. Rachinskii, and A. G. Vladimirov, "Bistability and hysteresis in an optically injected two-section semiconductor laser," Phys. Rev. E **89(5)**, p. 052903, 2014.
- [20] N. Rebrova, T. Habruseva, G. Huyet, and S. P. Hegarty, "Stabilization of Passively Mode-Locked Laser by Continuous Wave Optical Injection," Appl. Phys. Lett., **97**, pp. 101105-1–101105-3, 2010.
- [21] T. Habruseva, N. Rebrova, S. P. Hegarty, and G. Huyet, "Mode-Locked Semiconductor Lasers with Optical Injection," in *Quantum Dot Devices, Lecture Notes in Nanoscale Science and Technology* **13**, Springer-Verlag, NY, pp. 65–91, 2012.
- [22] E. Sooudi, G. Huyet, J. McInerney, F. Lelarge, K. Merghem, R. Rosales, A. Martinez, A. Ramdane, and S. Hegarty, "Optical Frequency Comb Generation Using Dual-Mode Injection-Locking of Quantum-Dash Mode-Locked Lasers: Properties and Applications," IEEE J. Quant. Electron. **48(10)**, pp. 1327–1338, 2012.
- [23] T. Habruseva, D. Arsenijevic, M. Kleinert, D. Bimberg, G. Huyet, and S. P. Hegarty, "Optimum phase noise reduction and repetition rate tuning in quantum-dot mode-locked lasers," Appl. Phys. Lett. **104(2)**, p. 021112, 2014.
- [24] A.G. Vladimirov, D. Turaev, and G. Kozyreff, "Delay differential equations for mode-locked semiconductor lasers," Opt. Lett. **29**, pp. 1221–1223, 2004.
- [25] A.G. Vladimirov and D. Turaev, "A new model for a mode-locked semiconductor laser," Radiophysics and Quantum Electronics **47**, pp. 769–776, 2004.
- [26] A. G. Vladimirov and D. Turaev, "Model for passive mode locking in semiconductor lasers," Phys. Rev A **72(3)**, p. 033808, 2005.

- [27] R. M. Arkhipov, A. Amann, and A. G. Vladimirov, "Pulse repetition-frequency multiplication in a coupled cavity passively mode-locked semiconductor lasers," Applied Physics B **118(4)**, p. 539, 2015.
- [28] N. Rebrova, G. Huyet, D. Rachinskii, and A. G. Vladimirov, "Optically injected mode-locked laser," Phys. Rev. E **83**, p. 066202, 2011.
- [29] A. Pimenov, T. Habruseva, D. Rachinskii, S. P. Hegarty, G. Huyet, and A. G. Vladimirov "Effect of dynamical instability on timing jitter in passively mode-locked quantum-dot lasers," Opt. Lett. **39(24)**, pp. 6815–6818, 2014.
- [30] L. Jaurigue, A. Pimenov, D. Rachinskii, E. Schöll, K. Lüdge, and A. G. Vladimirov "Timing jitter of passively-mode-locked semiconductor lasers subject to optical feedback: A semi-analytic approach," Phys. Rev. A **92**, p. 05380, 2015.